View metadata, citation and similar papers at core.ac.uk
brought to you by CORE
provided by Elsevier - Publisher Connector

Cell PRESS
Immunity
Article

HIV-1 Broadly Neutralizing Antibody Extracts Its Epitope from a Kinked gp41 Ectodomain Region on the Viral Membrane

Zhen-Yu J. Sun,[1,6] Kyoung Joon Oh,[2,4,6,7] Mikyung Kim,[2,5,6] Jessica Yu,[5] Vladimir Brusic,[2,4] Likai Song,[2,4] Zhisong Qiao,[2,5] Jia-huai Wang,[1,3,5] Gerhard Wagner,[1] and Ellis L. Reinherz[2,4,5,*]
[1]Department of Biological Chemistry and Molecular Pharmacology
[2]Department of Medicine
[3]Department of Pediatrics
Harvard Medical School, Boston, MA 02115, USA
[4]Cancer Vaccine Center
[5]Laboratory of Immunobiology and Department of Medical Oncology
Dana-Farber Cancer Institute, Harvard Medical School, Boston, MA 02115, USA
[6]These authors contributed equally to this work.
[7]Present address: Department of Biochemistry & Molecular Biology, Rosalind Franklin University of Medicine and Science, 3333 Green Bay Road, North Chicago, IL 60064, USA.
*Correspondence: ellis_reinherz@dfci.harvard.edu
DOI 10.1016/j.immuni.2007.11.018

SUMMARY

Although rarely elicited during natural human infection, the most broadly neutralizing antibodies (BNAbs) against diverse human immunodeficiency virus (HIV)-1 strains target the membrane-proximal ectodomain region (MPER) of viral gp41. To gain insight into MPER antigenicity, immunogenicity, and viral function, we studied its structure in the lipid environment by a combination of nuclear magnetic resonance (NMR), electron paramagnetic resonance (EPR), and surface plasmon resonance (SPR) techniques. The analyses revealed a tilted N-terminal α helix (aa 664–672) connected via a short hinge to a flat C-terminal helical segment (675–683). This metastable L-shaped structure is immersed in viral membrane and, therefore, less accessible to immune attack. Nonetheless, the 4E10 BNAb extracts buried W672 and F673 after initial encounter with the surface-embedded MPER. The data suggest how BNAbs may perturb tryptophan residue-associated viral fusion involving the mobile N-terminal MPER segment and, given conservation of MPER sequences in HIV-1, HIV-2, and SIV, have important implications for structure-guided vaccine design.

INTRODUCTION

Since the acquired immunodeficiency syndrome (AIDS) was recognized in 1981, an estimated 65 million infections and 25 million deaths have been ascribed to human immunodeficiency virus-1 (HIV-1) (CDC, 2006). Preventative vaccination is paramount to eliminate further global HIV-1 spread. Although clinically valuable T cell-based vaccines may be developed, B cell-stimulating vaccines capable of eliciting broadly neutralizing antibodies (BNAbs) are essential (Douek et al., 2006; Letvin, 2006). Only BNAbs will prevent entry of the HIV retrovirus into T cells to block viral replication as well as proviral integration into the host genome, the latter establishing latent reservoirs of disease (Han et al., 2007).

Unprecedented challenges to vaccine development arise from virtually every aspect of HIV-1 biology including the extraordinary viral sequence diversity of HIV proteins of which the virion surface gp160 spike protein is an example (Korber et al., 2001). gp160 is synthesized as a precursor, cleaved by furin-like enzymes in the transgolgi into gp120 and gp41 subunits that noncovalently associate, and assembled into heterotrimers. gp120 binds to cell-surface CD4, then undergoes conformational change revealing a coreceptor attachment site (Feng et al., 1996) whose ligation in turn induces structural rearrangements within the transmembrane gp41 subunit to fuse viral and host cell membranes (Chan et al., 1997). gp160 is extensively glycosylated, displays prominent variable loop segments, exists in several conformational states, and is proteolytically labile. These features engender antibody responses primarily directed against strain-specific sequences and including peptidic, non-native HIV epitopes. In contrast, little viral cross-species neutralizing activities are elicited against conserved structural elements that are shielded, difficult to access, or transient. Not surprisingly, therefore, only a handful of human BNAbs have been identified to date (reviewed in Douek et al., 2006). Those BNAbs with the greatest viral clade and strain breadth, including 2F5 and 4E10 (derived from immortalized B cells of HIV-1-infected individuals) and Z13e1 (selected from an affinity-matured phage-display library using bone marrow RNA derived from a clade B-infected individual), each targets the membrane-proximal ectodomain region (MPER) of gp41 (Nelson et al., 2007, and references therein). The MPER lies at the base of gp41, immediately proximal to the envelope's transmembrane segment, and although accessible to antibody, rarely, if ever, elicits BNAbs during natural infection.

Detailed structural analysis of the MPER on a lipid environment approximating native conditions is, therefore, of great

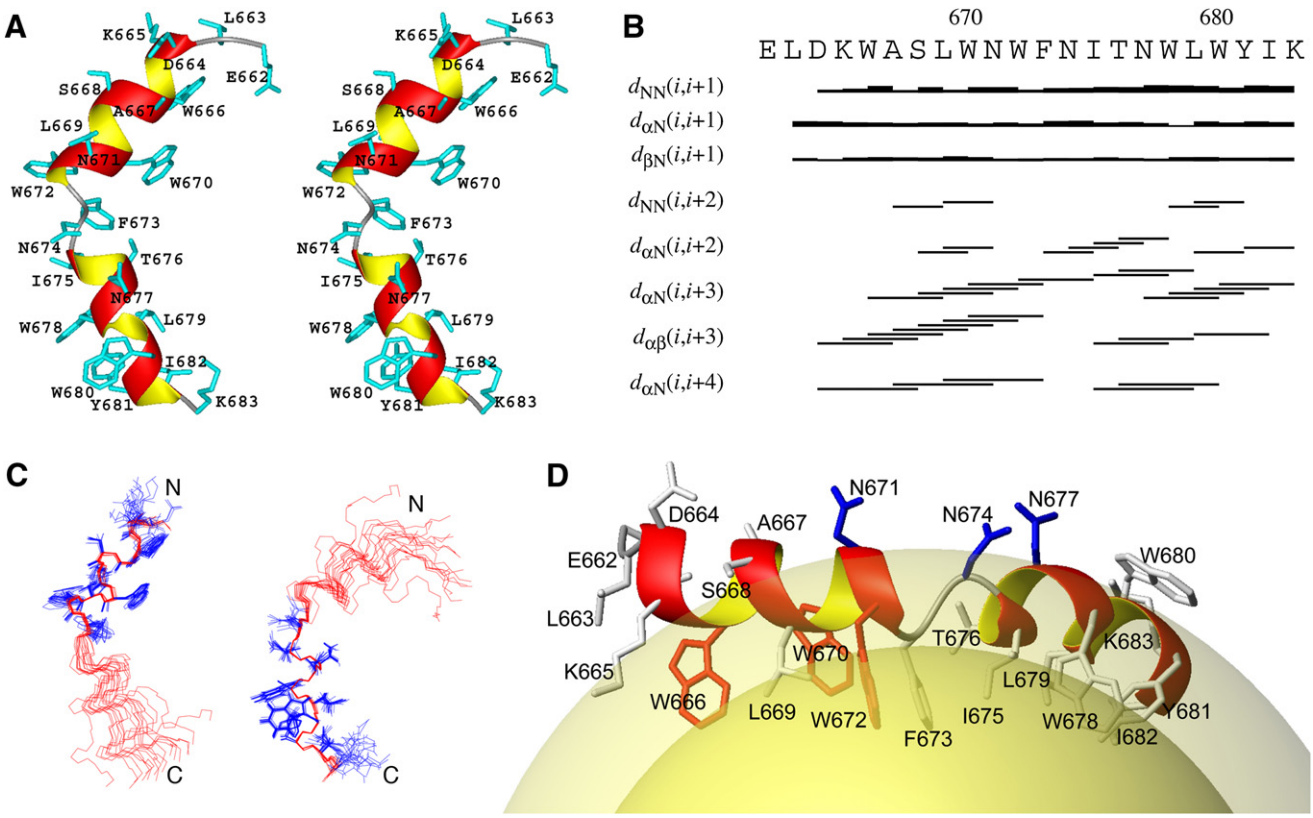

Figure 1. NMR Structure of the MPER in a DPC Micelle

(A) Stereo ribbon diagram of the MPER HxB2 peptide.

(B) Sequential plot of NMR constraints showing the α-helical pattern at the N-terminal and mixed 3_{10} and α-helical pattern at the C-terminal end of MPER peptide. This diagram is produced from CYANA (Guntert et al., 1992).

(C) Ensemble of 17 MPER NMR structure models superimposed by backbone atoms (colored in red) of the N-terminal segment (left in blue) or the C-terminal segment (right in blue).

(D) Placement of the MPER peptide on the micelle surface (light yellow spheres at the bottom). The deep yellow sphere represents the lipid acyl-chain region. The three well-conserved Trp residues important in virus-mediated fusion are shown in red, the three more variable solvent-exposed Asn residues are colored blue.

importance. In this regard, a recent cryoelectron microscopy study (Zhu et al., 2006) has yielded a 3-dimensional structure of the AIDS virus envelope spike, suggesting that each trimer has independent legs that project obliquely from the trimer head, like a tripod, and include the above BNAb region. Given the low resolution achieved in that report and substantial differences with a second tomographic study (Zanetti et al., 2006), we have determined at near atomic resolution the structure and disposition of the MPER on lipid membranes. In addition, we have characterized MPER conformational changes upon 4E10 monoclonal antibody (mAb) binding by using complementary nuclear magnetic resonance (NMR) and electron paramagnetic resonance (EPR) biophysical methods. The findings provided a structural rationale both for how BNAbs function to block HIV-1 infection and for improving HIV vaccine design to elicit them.

RESULTS

The Micelle-Bound MPER Adopts an L-Shaped Helical Structure

The HIV-1 MPER segment (amino acids 662–683) contains a large number of hydrophobic residues, and hence can be solubilized in aqueous solutions only in the presence of detergents or lipid vesicles. NMR spectroscopic studies of the HXB2 MPER in DPC micelles at pH 6.6 were carried out with isotopically labeled peptide and multidimensional triple-resonance experiments. The solution structure consisted of two discrete helical segments with a central hinge, forming an L-shape (Figure 1A). The N-terminal segment contained a 2-turn α helix from D664 to W672, whereas the C-terminal segment began with a 1-turn α helix from I675 to L679 followed by a 3_{10} helix from W680 to K683. The characteristic α-helical 3-residue separated Hα to Hβ NOE and 4-residue separated Hα to HN NOE were clearly missing for residues F673 and N674 in the hinge region (Figure 1B). The flexibility of the hinge region resulted in an overall backbone rmsd of 0.59 Å when superimposed from residues 665 to 682 (see Table S1 available online). However, the individual N- or C-terminal segments converged well, with backbone rmsd of 0.24 Å and 0.15 Å, respectively (Figure 1C), excluding the two N-terminal residues, E662 and L663, and the C-terminal K683, which appeared to be extended and unstructured.

This structure is distinct from the straight α helix of an earlier NMR model for the unlabeled MPER peptide in DPC micelle at pH 3.5 (Schibli et al., 2001), which does not present a single

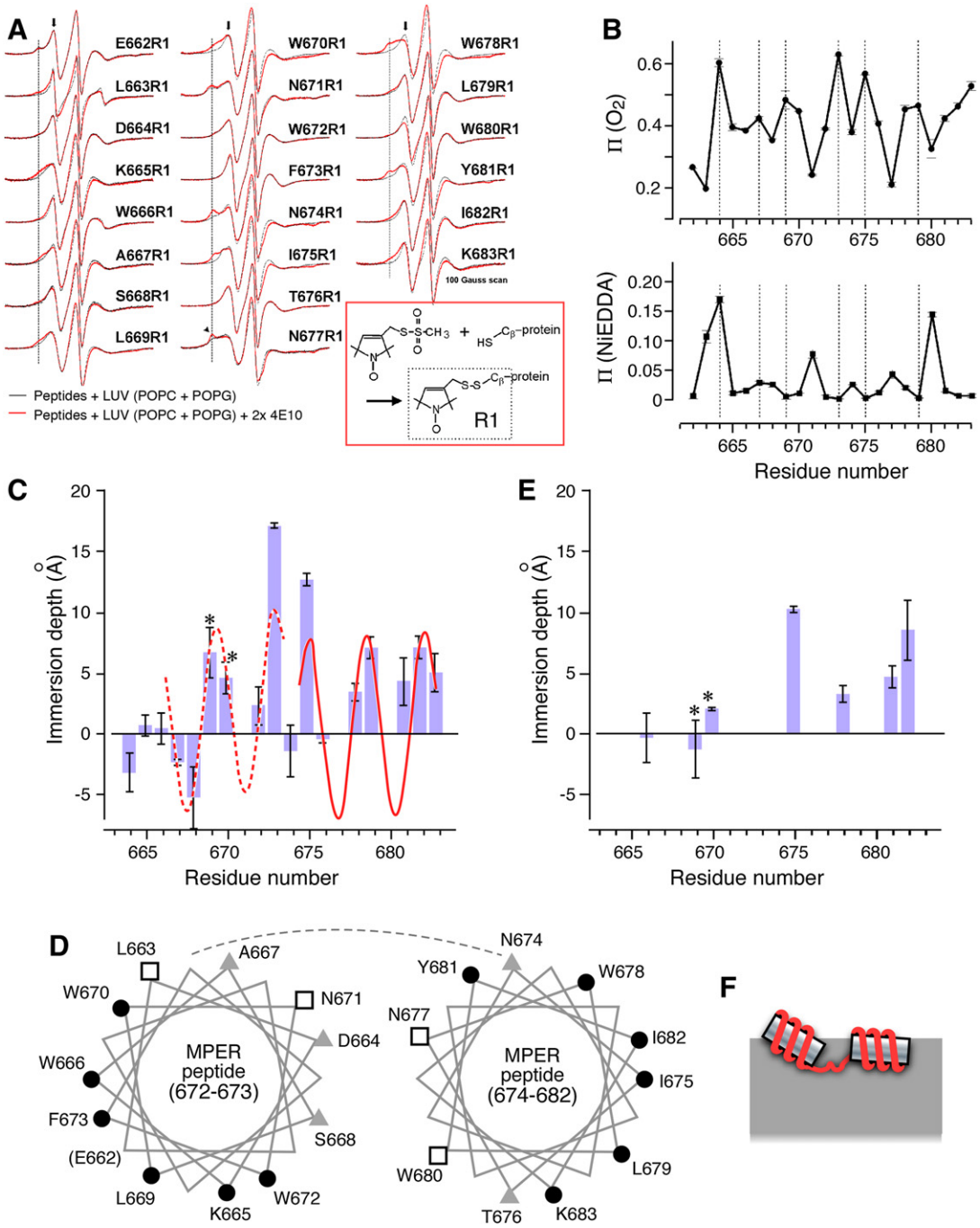

Figure 2. MPER Analysis by EPR: EPR Spectra, Accessibility Parameters, Immersion Depth, and Overall Topology

(A) EPR spectra of R1 side chains in MPER peptides bound to large unilamellar vesicles of POPC+POPG (4:1, w/w). Spectra were obtained in the absence (black trace) and presence (red trace) of 4E10 antibody twice in excess to the peptide. Characteristic features of highly mobile spectra (E662R1, W670R1, and W678R1) and highly immobile one (N677R1) are indicated by arrows and by an arrowhead, respectively. The vertical dotted lines indicate the approximate region of some spectra where the immobile components are increasing upon 4E10 binding. Scan width (abscissa) was 100 Gauss. Generation of the R1 side chain by the reaction of the methanethiosulfonate nitroxide spin label with the cysteine residue is shown in the inset.

(B) Accessibility parameters $\Pi(O_2)$ and Π(NiEDDA) for R1 residues in MPER peptides bound to POPC+POPG vesicles as a function of residue number. Air oxygen and 5 mM NiEDDA were used to measure the accessibility parameters, $\Pi(O_2)$ (top) and Π(NiEDDA) (bottom), respectively. The positions of $\Pi(O_2)$ maxima and corresponding positions in Π(NiEDDA) are marked with vertical dotted lines.

(C) Immersion depth of the lipid-facing R1 residues of MPER bound to POPC+POPG (4:1, w/w) vesicles. Average values of 2–3 independent measurements are reported with standard deviation. Depth values larger than 0 Å and between 0 and −5 Å correspond to acyl chain region and headgroup region in the membrane,

membrane-binding face. The kinked MPER structure with two separate helical segments, on the other hand, uniquely possesses a hydrophobic membrane-binding face containing 4 of the 5 Trp residues as well as the critical Phe 673 residue described below, while 3 hydrophilic Asn residues within the 4E10 epitope are solvent exposed (Figure 1D; Figure S1). Taken together, the L-shaped MPER structure on the membrane surface is largely determined by the primary sequence distribution of the hydrophobic amino acid residues.

Membrane Immersion Depths of Individual MPER Residues

To experimentally determine the orientation of the MPER in the membrane-bound state, we used the site-directed spin labeling method (Hubbell et al., 1998) of electron paramagnetic resonance (EPR) spectroscopy to study 22 synthetic MPER peptides with spin labels at different residue positions (Figure 2A). The accessibility values of the nitroxide spin-labeled side chains (R1) to the relaxation agents, oxygen and NiEDDA, were measured by power saturation techniques (Altenbach et al., 1994) for each spin-labeled peptide bound to a lipid bilayer (liposome) consisting of POPC and POPG molecules. The plots of accessibility parameters $\Pi(O_2)$ and Π(NiEDDA) (Figure 2B) showed that the collision frequencies of the spin-labeled side chain R1 for the relaxation agents oscillated as a function of sequence position. Hence, the spin labels alternated between polar and nonpolar environments. Interestingly, the two curves oscillated approximately in the same phase for residues 662R1–667R1 but in the opposite phase (180°) for residues 668R1–683R1. The periodicity with local maxima (or minima) often occurred at every third or fourth sequence position, suggesting that most residues were in helical conformation in the presence of membrane. The membrane immersion depths of MPER residues derived from the ratio of the accessibility parameters were determined by EPR as shown in Figure 2C. The residues L669R1, W670R1, W672R1, F673R1, I675R1, W678R1, L679R1, Y681R1, I682R1, and K683R1 were buried in the acyl chain region of the lipid bilayer (depth > 0 Å) while residues K665R1, W666R1, and T676R1 resided close to the interface between the acyl chain region and the lipid headgroup region. Residues D664R1, A667R1, S668R1, and N674R1 were in the phospholipids headgroup region (-5 Å $\leq$ depth $\leq$ 0 Å). Other residues such as L663R1, N671R1, N677R1, and W680R1 were completely exposed to the aqueous phase so that the immersion depths could not be determined. The accessibility parameters and the immersion depth data showed opposing solvent-exposed and membrane-interacting faces, which were out of phase on the two N- and C-terminal helices separated at residue N674 (Figure 2D), supporting the presence of a kink in the MPER helix.

To provide a detailed structural basis for the EPR results, the orientation of the MPER peptide relative to the lipid bilayer was determined by fitting the membrane immersion-depth data by computer simulations via simple helical models (Figure S2). As depicted in Figure 2C, the N-terminal segment of the peptide (residues 664–672) is in α-helical conformation with a tilting angle of approximately 15° (upwards at the N terminus) relative to the membrane surface (see also Figures 1D and 2F). The residues 662–666 in the N-terminal helical segment, however, didn't fit well with the predicted depth pattern (not shown), for which the accessibility parameters $\Pi(O_2)$ and Π(NiEDDA) oscillate approximately in the same phase (Figure 2B). This discrepancy may originate from either altered spin label conformations or from high exposure to the aqueous phase, as often observed for helices on a soluble protein surface (Hubbell et al., 1998). The C-terminal segment (residues 675–683) lies essentially parallel to the membrane surface (tilt angle less than 5°; Figure 2C; Figure S2). The two helical segments connect through a kink (Figure 2F) with angles ranging from 90° to 150° that were primarily defined by the peptide bonds between F673 and N674 (Figure 1C). The pivot residue N674 resided in the membrane headgroup region and pointed toward the aqueous phase. In contrast, F673 and I675, hydrogen-bonded within the N- and C-terminal helices, respectively, anchored deeply toward the hydrophobic region of the membrane (Figures 1D and 2C).

The immersion depths of MPER R1 residues bound to virus membrane-like liposomes (DOPC/SM/DOPE/DOPG/CHOL with the molar ratio of 34:7:16:10:33) showed essentially the same results (Figure S3A), suggesting that the kinked structure is a general feature even with a different lipid composition. In addition, the NMR analyses of ^{15}N-labeled MPER peptide in DPC micelle and disc-like DHPC-DMPC bicelle showed similar spectral patterns (Figure S3B). Because the MPER peptide bound to the flat surfaces of lipid bicelle that resemble the membranes of much larger lipid vesicles, the conformations of the MPER peptides were expected to be similar in the membrane systems (Chou et al., 2002) used in our EPR and NMR studies. It is important to note that the L-shaped structure was not caused by an adaptation of the peptide to the curvature of the micelle surface. Instead, a large portion of the kink region in the middle of the peptide was immersed deeply into the micelle (Figure 1D), while the N-terminus projected away from the micelle consistent with a trajectory connecting to the extracellular part of gp41 in the full-length protein. Overall, the N-terminal residues were predominantly exposed to the aqueous phase, whereas the C-terminal residues leading to the transmembrane helix were mostly immersed in the membrane.

respectively. The depths of lipid-facing R1 residues were fitted with membrane surface-bound helical models for the N-terminal (residues 667–673, dotted curve) and C-terminal (residues 676–682, solid curve) helices as described in Figure S2.

(D) Helical wheel diagrams for N-terminal (residues 662–673) and C-terminal (residues 674–682) segments of the membrane-bound MPER. Open square, shaded triangle, or filled circle represents a R1 residue exposed to aqueous phase, buried in the lipid headgroup region, or in the acyl chain region, respectively. The topological location of the residue in parentheses was not determined.

(E) Membrane immersion depth for R1 residues in membrane-bound and 4E10-bound MPER peptide. The depths of the indicated R1 residues in the MPER peptides bound to the POPC:POPG vesicles were measured in the presence of equimolar 4E10 antibody. Residues showing the largest depth change upon 4E10 binding are indicated with asterisks.

(F) A topological model of MPER peptide in the membrane (see also Figure S2). The tilted N-terminal helix (residues 664–672) is linked to the C-terminal helix (residues 675–683) lying almost parallel to the membrane surface. Residues 673–674 serve as a linker.

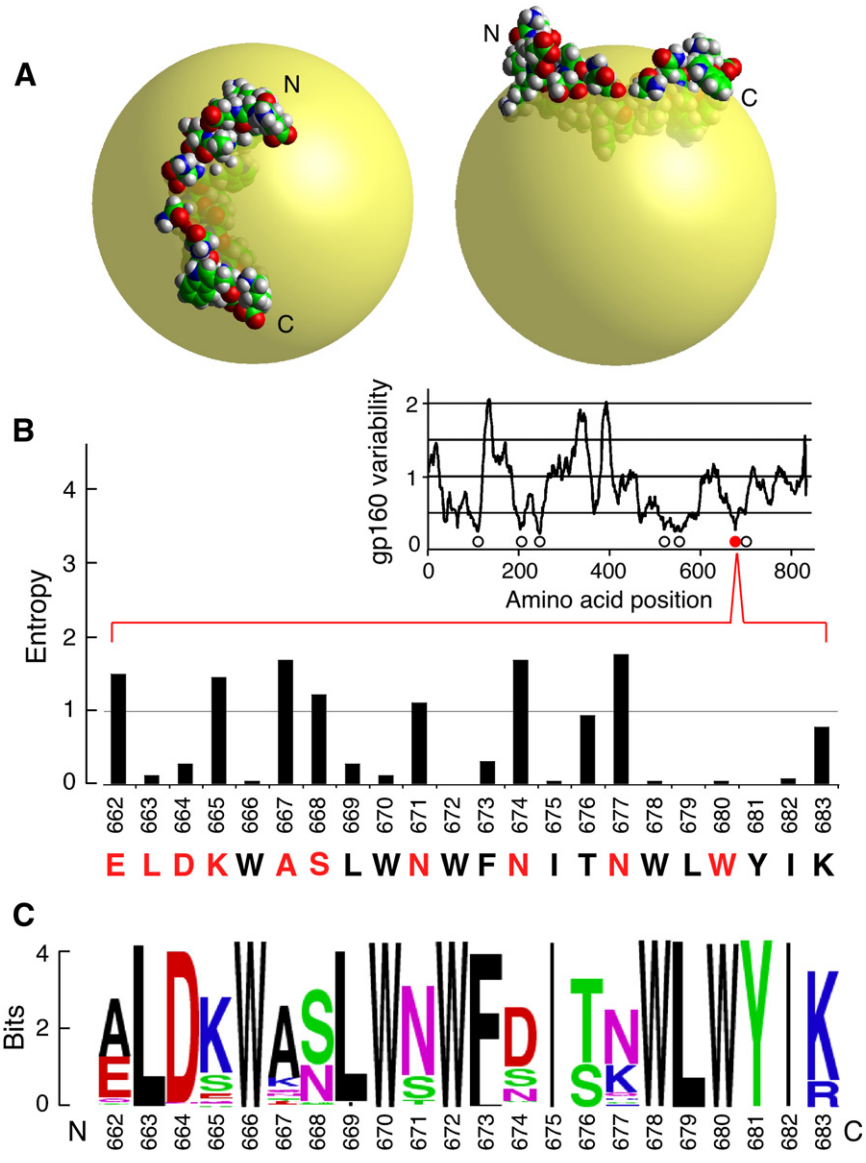

Figure 3. Sequence Conservation within the MPER Segment of HIV-1 Envelope Proteins

(A) Space-filling model of the HxB2 MPER peptide on a micelle (48 Å diameter).

(B) Shannon entropy is plotted for each residue from 975 HIV-1 sequences with variability on the *y* axis (0 = no variability at a given position; 4.322 = all 20 amino acids permitted at that position). The insert shows variability over the entire gp160 proteins from these same viral isolates. Open circles represent regions of conservation in gp160 comparable to that of the MPER segment (red dot) and correspond to amino acid residues (from left to right) 85–117, β1- α1 elements buried within the inner domain; 187–222, V2- β3- β4 largely buried segments; 230–258, LA β6- β8, LB, mostly buried within the inner domain; 512–534, fusion peptide; 553–590, the N leucine zipper; and 684–705, the TM segment abutting the MPER. Analyses were performed with a window size of 20 residues and with the *x* axis showing amino acid position of the window start. The residues that are solvent accessible are shown in red.

(C) Graphical representation of amino acid patterns within sequence alignments with WebLogo.

Exposed Residues Display Greatest Sequence Variability within the Conserved MPER

The space-filling models of the MPER reveal how it is largely immersed in a micelle (Figure 3A). Remarkably, hydrophobic residues buried in the lipid phase are the most conserved, in general, whereas those polar residues exposed to the aqueous phase are the most variable. As shown by Shannon entropy analysis of 975 HIV-1 sequences compiled from M, O, N, and U groups and available M subgroups (Figure 3B; Figure S4), the variability of amino acids at each of the 22 positions is limited, being among the least variable of all 20 amino acid segments probed within the gp160 molecule (Figure 3B, insert). In particular, the 15 C-terminal residues of the MPER include only three positions, 671, 674, and 677 with values ≥ 1. The other residues are either invariant or very restricted, primarily representing dimorphic variants (Figure 3C). Nonetheless, the implications of even this limited variability for vaccine design, as discussed later, are remarkable because subtle sequence alterations at 671 and/or 674 affect 4E10 and Z13e1 binding. Thus, it is evident that the hypervariability of the exposed residues as well as the immersion of conserved hydrophobic residues in lipid facilitate evasion of immune attack.

EPR Immersion Depth Changes upon 4E10 mAb Binding

Unexpectedly, both EPR and NMR results showed that three hydrophobic residues (W672, F673, and L679) critical for neutralization of the HIV virus by 4E10 mAb (Zwick et al., 2005) were buried in the lipid phase. Only the key polar T676 residue was in the headgroup region. These findings suggest that the 4E10 mAb first attached onto the membrane-bound MPER and subsequently induced a major conformational change in the peptide, exposing the complete epitope. To this end, we obtained EPR membrane immersion depth data on spin-labeled MPER peptides that retain affinity for 4E10 binding (Figure 2A; Figure S5) to confirm the orientation of the MPER peptide in complex with 4E10 mAb with respect to the membrane (Figure 2E). Spectral decomposition of the spectra of 669R1, 679R1, 675R1, 678R1, and 681R1 in the presence of equimolar 4E10 (not shown), which were essentially identical to those in Figure 2A, suggested that the peptides were in equilibrium between the free and bound state, obscuring accurate determination of the immersion depths of the antibody-bound peptide in the membrane. However, the change in the presence (Figure 2E) and absence (Figure 2C) of 4E10 could be used as an indicator of either the depth change or conformational change upon 4E10 binding for these residues.

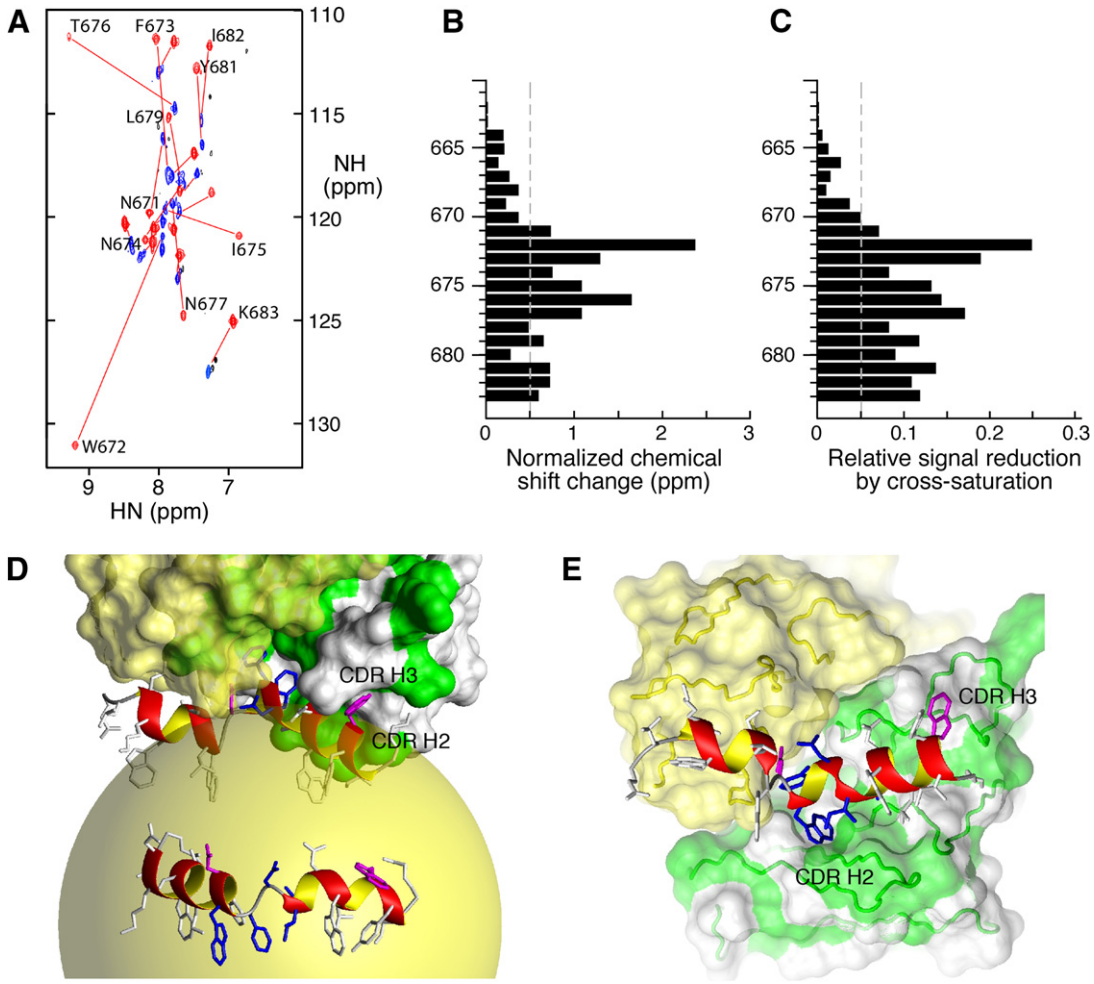

Figure 4. Conformational Change in MPER Induced by 4E10

(A) ^{15}N-TROSY-HSQC spectrum containing free (blue) and Fab-bound HxB2 MPER peptide (red).

(B) Normalized (sqrt((ΔHcs)^2 + (ΔNcs/5)^2) in ppm) MPER amide chemical shift changes upon 4E10 binding.

(C) Relative signal reduction of amide peaks with 250 ms cross-saturation showing MPER residues involved in 4E10 interaction.

(D and E) Models for MPER peptide in complex with 4E10 antibody as viewed from the side (D) and membrane face (E). The 4E10 light chain is colored yellow, and the hydrophobic patches on 4E10 heavy chain are colored in green. The residues W672 to T676 essential for 4E10 binding are shown in blue, and residues N671 and W680 important for initial contacts with CDR3L and CDR3H, respectively, are shown in pink. In (D), the orientation of uncomplexed MPER is shown for comparison.

Note that the EPR spectral changes were highly specific to the 4E10 antibody and the MPER peptide sequence as shown by data derived from negative controls consisting of a 4E10-unreactive mutant peptide W672A:F673A:N677R1 and a nonbinding control IgG antibody (Figure S6). Notably, pronounced EPR spectral changes were observed in N674R1, I675R1, N677R1, W678R1, and Y681R1 (Figure 2A), at or near the C-terminal end of the MPER peptide. On the other hand, the spin labeling at positions W672, F673, and T676 completely abolished 4E10 antibody binding as determined by surface plasmon resonance (SPR) experiments, and resulted in little or no EPR spectral changes in the presence of 4E10 (Figure 2A; Figure S5). Overall, the trends in the change in the immersion depth data implied that the N-terminal segment was lifted up toward the aqueous phase whereas the C-terminal segment was little affected (Figure 2E).

MPER Conformational Changes upon 4E10 mAb Binding

To confirm those structural changes and assess conformational alterations at all key binding residues, we investigated the MPER peptide in complex with the 4E10 antigen-binding fragment (Fab) in deuterated DPC micelles by NMR spectroscopy. The amide chemical shift perturbations of the MPER residues upon 4E10 binding are shown in Figures 4A and 4B. Although all residues that were measured manifest noticeable peak shifts, the residues displaying the most significant changes (>0.5 ppm of normalized chemical shifts) included the core 4E10 epitope residues WFNIT (672–676), plus residues N671, N677, and L679, and the three C-terminal residues Y681, I682, and K683. Results from NMR cross-saturation experiment further identified those residues in direct contact with the 4E10 antibody, because NMR magnetizations are transferred from the protonated methyl regions of 4E10 to the

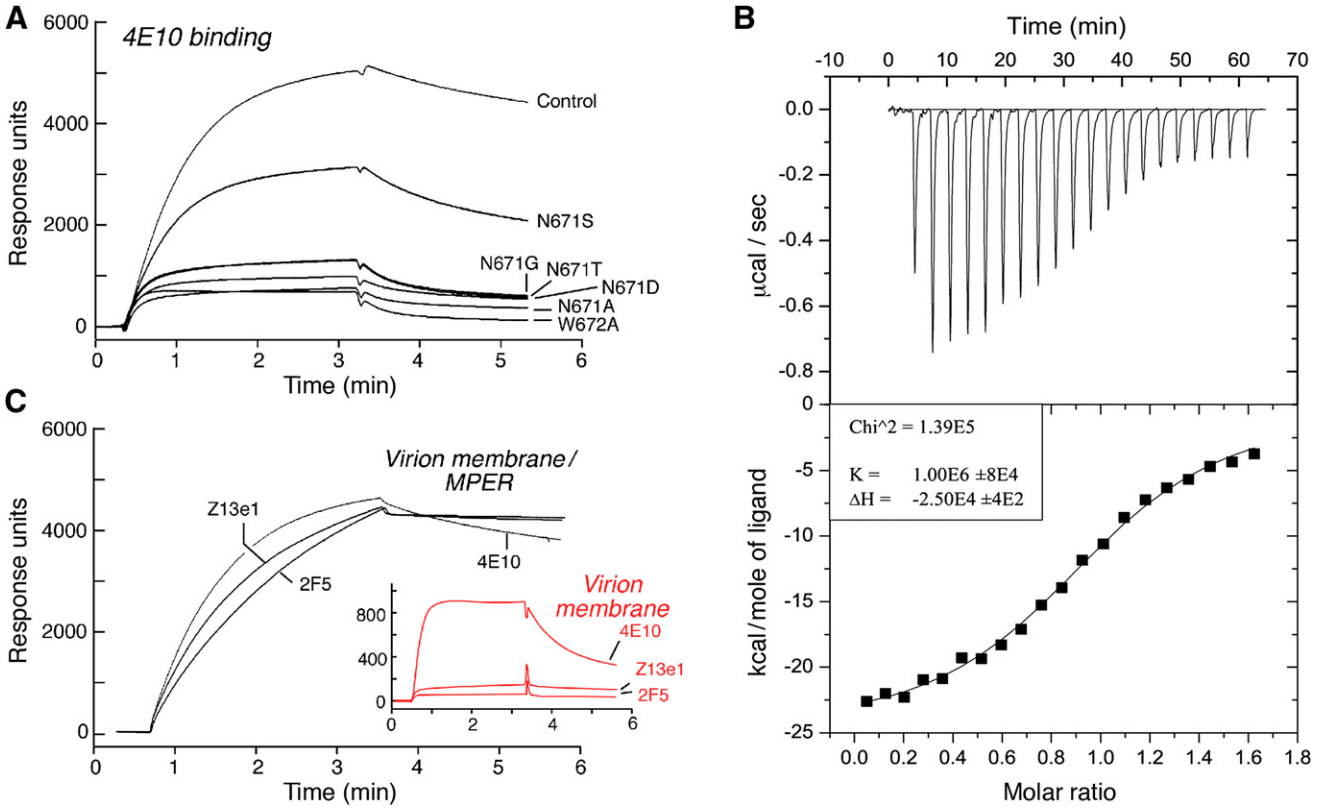

Figure 5. Assessment of BNAb with Membrane and MPER

(A) Critical role of N671 for 4E10 binding to MPER and liposomes by BIAcore. Control (HXB2) MPER and single amino acid variants are shown. 2F5 reactivity for each variant was equivalent to the HXB2 control (not shown).

(B) ITC result of injecting 250 μM of MPER peptide with virion membrane-like liposome into 10 μM 4E10 Fab at 25°C. The enthalpy change is −25.0 kcal/mole of Fab molecule and the binding constant is 1.0 μM from fitting results, yielding a large positive entropic energy change of (−TDS) = 16.9 kcal/mole.

(C) Binding of BNAbs 4E10, 2F5, and Z13e1 to synthetic virion membrane-bound MPER (virion membrane+MPER) (black) and virion membrane alone (red insert).

nearby amides of the per-deuterated MPER peptide. The residues in the MPER peptide that showed cross-saturation change (>5% reduction) include the C-terminal segment 671–683 (Figure 4C).

The region of MPER peptide responsible for 4E10 binding, therefore, was not restricted to the WFNIT core but comprised a segment spanning ~18 Å, consistent with the width of the 4E10 Fab binding site. These results obtained for 4E10 binding in the presence of membrane are in general agreement with the recently published crystal structure of a soluble shorter (671–683) MPER peptide in complex with the 4E10 antibody (Cardoso et al., 2007).

Modeling 4E10 Interaction with the Micelle-Bound MPER

The combined NMR and EPR data refined the existing model of the 4E10 in complex with the full-length MPER peptide. Secondary structure information was obtained from the ^{13}C chemical shifts values of the per-deuterated MPER peptide in complex with 4E10 (Figure S7 and Table S2). Upon binding, the hinge region in the kinked MPER peptide had become part of the C-terminal helix from W672 to K683, and residues W670 and N671 adopted an extended, nonhelical conformation, in agreement with the crystal structure (Cardoso et al., 2005, 2007). The N-terminal segment remained α-helical from residues D664 to L669, permitting this segment to be appended to the shorter MPER peptide from the crystal structure by overlapping the residues N671 and W672 in our model (Figures 4D and 4E). The NWFNIT segment made extensive interactions with antibody, with F673 swinging upward ~15 Å (end-to-end) and inserting deeply into the 4E10 binding pocket. Additional contacts were contributed by residues L679, W680, I682, and K683. Among the four MPER residues (N671, N674, N677, and W680) that were solvent accessible in the free form, N671 was the most important for 4E10 interactions, by forming a hydrogen bond with the 4E10 light chain (Cardoso et al., 2005, 2007).

N671 likely participated in the initial contact between the 4E10 antibody and the lipid-embedded segment prior to MPER rearrangement as shown by the SPR data with a N671A mutant (Figure 5A). Consistent with this notion, N671A contributed little, if any, to 4E10 binding to MPER peptide in solution because other core residues including W672 and F673 were exposed (Brunel et al., 2006). Furthermore, mutation of N671 to naturally occurring residues in other viral strains moderately (N671S) or even more substantially (N671G, N671T, N671D) decreased 4E10 binding to the lipid-embedded MPER. Not surprisingly, envelopes from primary HIV-1 isolates with N671T mutation, for

example, with or without additional changes outside the 4E10 core epitope show up to a 10-fold greater 4E10 resistance in pseudovirus neutralization assays (Binley et al., 2004; Li et al., 2005). Upon antibody binding, the N-terminal helix prior to N671 remained relatively mobile, although partially confined by the 4E10 light chain positioned above the membrane. Based on the EPR results, the orientation of the 4E10 antibody was such that it tilts away from the MPER peptide allowing the hydrophobic CDR2 (and potentially CDR3) loop of the heavy chain fragment to set anchor in the viral membrane (Figures 4D and 4E). Collectively, 4E10 BNAb extracts its epitope from the viral membrane in a multistep process as depicted in Movies S1 and S2.

Strong Lipid Binding Is Not an Essential BNAb Requirement

To examine the energetics of 4E10 binding to the membrane-embedded MPER, we performed ITC and SPR experiments by using liposomes whose lipid constituents mimic those found in HIV-1 virions (Brügger et al., 2006). The enthalpy change by ITC was determined to be −25 kcal/mole for the Fab form of 4E10, with a 1.0 μM Kd, suggesting a high entropic energy penalty (Figure 5B). In addition, there was detectable monovalent binding of 4E10 Fab with the virion membrane-like liposome in the ITC experiment but too weak to quantitate. As a consequence, we examined intact BNAb IgG binding by SPR. Consistent with a prior study (Alam et al., 2007), the best global curve fitting of 4E10 binding to the membrane-bound MPER involved a two-step conformational change model with Kd of ~10 nM. Figure 5C compares the binding of 4E10 as well as Z13e1 and 2F5 to the virion membrane-embedded MPER versus virion membrane alone. As shown, specific binding of Z13e1 and 2F5 to the MPER was comparable to that of 4E10, but little or no direct binding to the membrane alone was observed. 4E10 mAb bound to the virion membrane mimic but with a much faster off-rate and, consequently, a much weaker affinity (~10 μM Kd). Thus, strong membrane binding was not an essential BNAb characteristic.

DISCUSSION

Biophysical studies demonstrate that the tryptophan-rich MPER peptide addition to liposomes results in membrane instability at high peptide concentrations (Lorizate et al., 2006). Tryptophan is well known for its role in membrane destabilization (Popova et al., 2002). Functional mutagenesis further highlights the important role of the MPER in HIV-1-mediated fusion (Dimitrov et al., 2007; Lorizate et al., 2006; Munoz-Barroso et al., 1999; Salzwedel et al., 1999; Suárez et al., 2000). Alanine substitutions of all five MPER W residues [W(1-5)A] or the three within the N-terminal helix (W666A, W670A, W672A) abrogates syncitium formation as does deletion of the core hinge area (Δ671–677) through inhibition of fusion pore expansion (Salzwedel et al., 1999). By contrast, N-terminal Δ666–670 or C-terminal Δ678–682 deletions reduce but do not eliminate syncitium formation, and the W678A, W680A double mutant of the MPER C-terminal helix W residues is without effect. The kink observed in the MPER peptide structure may serve to allow independent movement of the N-terminal segment containing the three W residues (W666, W670, and W672) critical for fusion (Figure 1D), relative to the more fixed C-terminal segment. These movements appear to be crucial for stable pore formation as suggested by earlier site-directed mutation analysis of MPER residues (Munoz-Barroso et al., 1999). In that study, scrambling the sequence shown in our current study to comprise the hinge and several flanking residues inhibited syncitium formation and macromolecular dye transfer but not small-molecule transfer between envelope-expressing cells and target cells. By modifying the membrane orientation and/or positions of the tryptophans, it is likely that 4E10 mediates its neutralizing activity, either by destabilizing the virus membrane and/or by impeding the sequence of conformational changes within the MPER region necessary to mediate virus-host cell fusion. Such neutralization is less likely to be via disruption of the six-helix bundle formation because other equally high-affinity mAbs targeting the C helix are not neutralizing (Alam et al., 2007).

The fact that 4E10 (core epitope W672-T676), 2F5 (core epitope D664-W666), and Z13e1 (core epitope W666-N677) all crossblock each other and are broadly neutralizing HIV mAbs further emphasizes the importance of this area (Barbato et al., 2003). Based on the tripod-like model of the HIV-1 spike, the MPER region is in a somewhat open configuration on the "foot" of "splayed leg" allowing access for these antibodies (Zhu et al., 2006). Perhaps the limited copy number of envelope protein on each HIV virion relative to orthologs on other type I fusion viruses requires the MPER to augment fusion pore formation, through stronger interaction with a larger membrane area. The current L-shaped tryptophan-rich MPER structure supported this picture. The 8-residue MPER segment C-terminal to the kink was likely to maintain a rigid association with the transmembrane domain, and probably involved in additional interaction with cholesterol in the lipid phase (Epand et al., 2006).

This report revealed how an epitope buried in the membrane can be recognized by an antibody. We demonstrated experimentally that the MPER undergoes major conformational change upon 4E10 binding in the lipid environment. Residue F673 swung 180° from the membrane interior to the antibody binding pocket analogous to DNA helix bending and base-flipping of nucleotides during DNA repair (Hollis et al., 2000). This dynamic process is a unique phenomenon for antibody recognition. The intrinsically flexible hinge and metastability of the MPER structure are important for this conformational change and could conceivably be involved in facilitating the viral membrane fusion process by disrupting the lipid layer of the opposing membrane from the host cell. BNAbs 4E10 and Z13e1 straddle this hinge, extracting key membrane-embedded residues into the antibody-combining site to achieve tight binding while dysregulating the involvement of the N-terminal segment in membrane destabilization.

Whereas the conformation of the 4E10 segment is presumed to be largely helical in both prehairpin and intermediate states, the conformational variability of the 2F5 segment may be greater (Ofek et al., 2004, and references therein). It is possible that the 2F5 segment of MPER may adopt a different conformation, if the 2F5 core or N-terminal adjacent sequence interacts with other envelope ectodomain elements. Notably, the N-terminal part of the 2F5 binding segment (662–663) and the hinge involving

4E10 and Z13e1 (673–674) appeared to be flexible in our structure. Similar to 4E10, 2F5 antibody may also extract its complete epitope after initial contact with key exposed residues (662–664). In addition, given that the gp41 6-helix bundle involves the 2F5 epitope sequence, 2F5 may also mediate neutralization by preventing hairpin formation from a prehairpin gp41 configuration. 4E10 and Z13e1 may disrupt MPER pore formation, expansion, or both processes.

That 4E10 and Z13e1 have comparable affinity for gp41 and peptide derivatives therein, yet 4E10 is considerably more biologically potent than Z13e1, argues that antibody affinity per se is not the single determinant of neutralization (Nelson et al., 2007). Consistent with this notion, the HIV-1 envelope trimer-reactive 13H11 mAb maps N-terminal to 2F5 and, although crossblocking the latter, is not a neutralizing antibody despite comparable 9–12 nM affinity (Alam et al., 2007). Induction of structural rearrangement of the MPER hinge region by antibodies seems to be a key requirement for neutralization, assuming equivalent accessibility to the segment. Consequently, it is possible that the broadly neutralizing antibodies act by targeting the flexible region so as to restrict the movements of the MPER peptide relative to other parts of gp41 during fusion-associated conformational changes.

The observation that 2F5 and 4E10 mAbs manifest reactivity to lipid autoantigens such as cardiolipin has raised the possibility that the scarcity of broadly neutralizing antibodies in humans may result from their elimination through natural B cell tolerance mechanisms to self-antigens (Alam et al., 2007; Haynes et al., 2005). The current structural data suggest that the lipid specificity of those BNAbs is a consequence of the membrane-embedded environment of the MPER against which they are elicited. The majority of binding energy is dependent on the unique MPER viral sequence, making it evident that viral-specific binding to the MPER rather than broad autoreactivity should be engendered from MPER-related immunogens. On the other hand, membrane lipid components may modulate MPER interaction with the membrane and/or with antibody, explaining, at least in part, the discrepancy in 4E10 antibody neutralization efficiency for the same virus produced in 293T cells versus peripheral blood mononuclear cells (Binley et al., 2004).

The binding of MPER peptide by 4E10 antibody may involve three steps as eluded to earlier. First, 4E10 antibody interacts with membrane and encounters the membrane-bound MPER peptide. The initial interaction likely involves N671, and possibly W680, thereby orienting the peptide with respect to the antibody binding pocket. In the second step, changes in the local peptide environment introduced by the hydrophobic regions of the antibody cause rearrangement of multiple side chains in the C-terminal segment. Especially, F673 may be rotated into the antibody binding pocket, concomitant with the backbone angle changes of F673 and N674 removing the kink in the middle of the peptide. In the third step, the insertion of F673 and W672 deep into the 4E10 binding pocket changes the backbone angles of W672, N671, and W670, bending the N-terminal segment in the opposite direction to avoid steric clashes with the 4E10 light chain.

In addition to being the target of existing monoclonal BNAbs with greatest breadth (Binley et al., 2004; Nelson et al., 2007), two immunogenicity studies underscore the importance of defining the MPER structure on a lipid environment for purposes of vaccine design. First, it has been observed that no HIV-1 BNAbs were elicited after immunization of animals with a truncated prefusion-envelope protein lacking the MPER (Qiao et al., 2005). Second, immunization of guinea pigs with recombinant HIV-1 virus-like particles (VLP) including the MPER-elicited high-titer VLP antibodies, but these were directed away from the MPER, instead showing specificity for the C-terminal helix segment of gp41 and without neutralizing activity (Kim et al., 2007). The lipid-embedded ''stealth'' feature of the MPER explains the lack of immune responses to the MPER as compared to more accessible immunodominant cluster I and II regions of gp41 (Xu et al., 1991). Thus, antibodies directed against the MPER 4E10 and 2F5 epitopes are rarely, if ever, found during natural infection and are extremely difficult to elicit through immunization because of the nonimmunodominance of this region (Kim et al., 2007; Yuste et al., 2006). Instead, non-neutralizing cluster I-II antibodies develop during HIV-1 infection.

Attempts to engineer enforced MPER helices, either engrafted on proteins (Law et al., 2007) or chemically stabilized by non-natural peptide bonds (Brunel et al., 2006; Cardoso et al., 2007), represent elegant approaches. However, the conformational changes noted within the lipid-embedded MPER upon 4E10 antibody binding to membranes dispelled the notion of a static ''neutralizing'' versus ''non-neutralizing'' MPER face for immunogen design. Vaccine design based on targeting postconformational change epitopes could misguide the immune system. Our structural data and bioinformatics analyses suggested that an appropriate solution may be the use of lipid-coated nanoparticles to present membrane-embedded MPER segments in their L-shaped native conformation displaying exposed 671, 674, and 677 variants and invariant residue 680 to the immune system. Such a strategy avoids exposure to exosomal proteins incorporated into VLPs or other misdirecting epitopes on chimeric proteins, instead allowing the isolated MPER to assume a native configuration in the lipid environment. By eliciting antibodies that contact the invariant exposed W680, in addition to the three polar exposed residues, it should be possible to engender high-affinity antibody interactions without a need to recruit buried residues, thereby avoiding entropic penalty. Our prediction is that such antibodies will be able to recognize native HIV-1 epitopes in the membrane environment, and bind the MPER with sufficient affinities to impede its fusogenic activity. Aside from providing impetus for future vaccination strategies, these data emphasize that BNAbs are notable for their site-specific binding to a functionally important envelope segment.

EXPERIMENTAL PROCEDURES

Materials

Phospholipids 1,2-dioleoyl-*sn*-glycero-3-phosphatidylcholine (DOPC), 1,2-dioleoyl-*sn*-glycero-3-phosphatidylethanolamine (DOPE), 1,2-dioleoyl-*sn*-glycero-3-[phospho-*rac*-(1-glycerol)] (DOPG), and egg sphingomyelin (SM) dissolved in chloroform and cholesterol (CHOL) in powder were purchased from Avanti Polar Lipids. 1-Palmitoyl-2-oleoyl-*sn*-glycero-3-phosphocholine (POPC), 1-palmitoyl-2-oleoyl-*sn*-glycero-3-[phospho-*rac*-(1-glycerol)] (POPG), 1-palmitoyl-2-oleoyl-*sn*-glycero-3-phosphotempocholine (PC tempo), 1-palmitoyl-2-stearoyl(5-doxyl)-*sn*-glycero-3-phosphocholine (5-doxyl PC), 1-palmitoyl-2-stearoyl(7-doxyl)-*sn*-glycero-3-phosphocholine (7-doxyl PC), 1-palmitoyl-2-stearoyl(10-doxyl)-*sn*-glycero-3-phosphocholine (10-doxyl PC),

and 1-palmitoyl-2-stearoyl(12-doxyl)-*sn*-glycero-3-phosphocholine (12-doxyl PC) were purchased from Avanti Polar Lipids, Inc. N-tempoylpalmitamide was synthesized as described (Shin and Hubbell, 1992). Dodecyl phosphatidylcholine (DPC) for micelle, 1,2-diheptanoyl-sn-glycero-3-phosphocholine (DHPC) and 1,2-Dimyristoyl-sn-Glycero-3-Phosphocholine (DMPC) for bicelle were purchased from Avanti Polar Lipids (Alabaster, AL). Deuterated (d38-) DPC was purchased from Cambridge Isotope Laboratories (Andover, MA). The MPER segment 662–683 of HXB2 (ELDKWASLWNWFNITNWLWYIK), the ADA strain (ALDKWASLWNWFDISNWLWYIK) or mutant variants were expressed as a GB1-MPER fusion protein in *E. coli*. Each peptide was released from the fusion protein via cyanogen bromide (CNBr) cleavage and purified by high-performance liquid chromatography (HPLC) to greater than 95% homogeneity. For spin-labeling experiments, the MPER segment 662–683 of HXB2 with a single cysteine substitution at various positions were synthesized and desalted at the Tufts Peptide Synthesis Core. The N and C termini of all the peptides were modified by acetylation and amidation, respectively.

EPR Spectroscopy

EPR spectra were obtained on a Bruker EMX spectrometer with a Bruker High Sensitivity resonator at room temperature. All spectra were recorded at 2 mW incident microwave power with a field modulation of 1.0–2.0 G at 100 kHz. For power saturation experiments, NiEDDA was synthesized as described (Altenbach et al., 1994; Oh et al., 2000). In order to measure the accessibility parameters, Π, of O_2 and NiEDDA, power saturation experiments were carried out with a loop-gap resonator (JAGMAR, Krakow, Poland) (Farahbakhsh et al., 1992; Oh et al., 2000; Shin and Hubbell, 1992). The source of oxygen gas was air supplied in-house and the concentration of NiEDDA was 5 mM. N_2 gas was used to purge O_2 when necessary. In order to measure the immersion depths of membrane-inserted spin-labeled residues (Supplemental Experimental Procedures), air O_2 and 50 or 100 mM NiEDDA were used as collision reagents. The range of the incident microwave power was 0.4 to 100 mW for power saturation experiments. Power saturation data were analyzed with the R program (version 1.5.1) (Ihaka and Gentleman, 1996). Depth calibration curves were determined with the large unilamellar vesicles consisting of POPC/POPG (4:1, w/w) containing spin-labeled lipids (see Supplemental Data) (Altenbach et al., 1994; Farahbakhsh et al., 1992) in the presence and absence of 4E10 antibody at 800:1 molar ratio of total phosphate to antibody. In order to determine the number of spin labels attached to peptides, EPR spectra were taken after liberating the spin labels from the peptide molecules by incubating the labeled peptides with 100 mM tris-(2-carboxyethyl)phosphine (Molecular Probes, Inc.). The amount of spin label was calculated by double integration of the EPR spectra with 3-carboxy-proxyl (Sigma-Aldrich) as a standard.

SPR Measurements

BIAcore experiments were carried out with a BIAcore 3000 with the Pioneer L1 sensor chip composed of alkyl chains covalently linked to a dextran-coated gold surface (BIAcore AB, Uppsala, Sweden) at 25°C. The running buffer was 20 mM HEPES containing 0.15 M NaCl (pH 7.4) (HBS-N). The BIAcore instrument was cleaned extensively and left running overnight with Milli-Q water to remove trace amounts of detergent. The LUV (30 μl, 5 mM) was applied to the sensor chip surface at a flow rate of 3 μl/min, and the liposomes were captured on the surface of the sensor chip and provided a supported lipid bilayer. To remove any multilamellar structures from the lipid surface, sodium hydroxide (20 μl, 25 mM) was injected at a flow rate of 100 μl/min, which resulted in a stable baseline corresponding to the immobilized liposome bilayer membrane with response units (RU) of 8,000–11,000.

Peptide solutions (0.7 μM) were prepared by dissolving in running buffer right before injection and the solution (60 μl) was injected over the lipid surface at a flow rate of 5 μl/min. Antibody solution (20 μg/ml) was passed over peptide-liposome complex for 3 min at a flow rate of 5 μl/min. Because the peptide-lipid interactions are very hydrophobic, the regeneration of the liposome surface was not possible. The immobilized liposomes were therefore completely removed with an injection of 40 mM CHAPS (25 μl) at a flow rate of 5 μl/min, and each peptide injection was performed on a freshly prepared liposome surface.

For analysis of antibody binding to spin-labeled, membrane-bound MPER peptides, a volume of 30 μl of POPC/POPG (4:1, w/w) LUVs (10.5 mM phosphate) in HBS-N was layered onto an L1 Sensor Chip and followed by spin-labeled peptide and antibody injection as described above at a rate of 3 μl/min. The wild-type and mutant peptide with 672A:673A double alanine substitution mutations were prepared as described in Expression and purification of MPER segments.

ITC Experiments

Samples for ITC experiments were prepared in HBS-N buffer. 20 injections of 15 μl liposome-MPER peptide mixture were delivered to 1.35 ml of 10 μM 4E10 Fab. 4E10 Fab was prepared with the Pierce Fab digestion kit according to the manufacturer's recommendations. Data were acquired at 25°C with a MicroCal ITC instrument and analyzed with the software Microcal Origin (Northampton, MA).

NMR Spectroscopy and Structure Modeling

Samples for NMR experiments were prepared by codissolving lyophilized MPER peptides with regular or deuterated DPC and adjusted to pH 6.6. All NMR experiments were carried out at 35°C on spectrometers equipped with cryogenic probes. The data for backbone assignment of MPER peptide in DPC micelle were acquired with a Varian Inova 600 MHz spectrometer. The 3D ^{15}N-NOESY (60 ms mixing time) and 2D NOESY (80 ms mixing time, in D2O) data were acquired with Bruker 750 MHz and 600 MHz spectrometers, respectively. The TROSY data of MPER peptide in complex with 4E10 Fab were acquired with a Bruker 900 MHz spectrometer. The cross-saturation experiment (Shimada, 2005) was performed on a Bruker 600 MHz spectrometer in an interleaved fashion with 250 ms WURST ^{1}H saturation pulses with 2.3 ppm bandwidth irradiating at 0 ppm (methyl region) and −40 ppm (empty region) for alternating FIDs.

Data were processed with the software PROSA (Guntert et al., 1992) and analyzed with the software CARA (Keller, 2004). Chemical shift assignments were carried out with conventional NMR techniques (Ferentz and Wagner, 2000). The preliminary structures were calculated with the software CYANA (Guntert, 2004) and the final structures by XPLOR-NIH (Brunger, 1992; Schwieters et al., 2003). NMR constraints and structural statistics are listed in Table S1.

The antibody-bound MPER peptide was modeled based on the X-ray crystallographic structure of peptide mimics in complex with 4E10 Fab (PDB code: 2FX7, 1TZG), the solution NMR structure of the free peptide as well as structural information obtained from the TROSY NMR experiments (Pervushin, 2000). The secondary structures were confirmed from TALOS (Cornilescu et al., 1999) analysis of the chemical shift data (Table S2).

Supplemental Data

Seven figures, two tables, two movies, and Experimental Procedures are available at http://www.immunity.com/cgi/content/full/28/1/52/DC1/.

ACKNOWLEDGMENTS

This work was supported by NIH grant AI43649 to E.L.R. and G.W. We thank M. Zwick and D. Burton for providing Z13e1 mAb, G. Heffron for supporting NMR experiments, M. Adamowicz and J. West for technical support, and L. Walensky and Y.-K. Shin for helpful discussions. Maintenance and operation of the NMR instruments used were supported by NIH grants GM47467 and EB2026.

Received: November 14, 2007
Accepted: November 27, 2007
Published online: January 10, 2008

REFERENCES

Alam, S.M., McAdams, M., Boren, D., Rak, M., Scearce, R.M., Gao, F., Camacho, Z.T., Gewirth, D., Kelsoe, G., Chen, P., and Haynes, B.F. (2007). The role of antibody polyspecificity and lipid reactivity in binding of broadly neutralizing anti-HIV-1 envelope human monoclonal antibodies 2F5 and 4E10 to glycoprotein 41 membrane proximal envelope epitopes. J. Immunol. *178*, 4424–4435.

Altenbach, C., Greenhalgh, D.A., Khorana, H.G., and Hubbell, W.L. (1994). A collision gradient method to determine the immersion depth of nitroxides in

lipid bilayers: application to spin-labeled mutants of bacteriorhodopsin. Proc. Natl. Acad. Sci. USA *91*, 1667–1671.

Barbato, G., Bianchi, E., Ingallinella, P., Hurni, W., Miller, M., Ciliberto, G., Cortese, R., Bazzo, R., Shiver, J.W., and Pessi, A. (2003). Structural analysis of the epitope of the anti-HIV antibody 2F5 sheds light into its mechanism of neutralization and HIV fusion. J. Mol. Biol. *330*, 1101–1115.

Binley, J.M., Wrin, T., Korber, B., Zwick, M.B., Wang, M., Chappey, C., Stiegler, G., Kunert, R., Zolla-Pazner, S., Katinger, H., et al. (2004). Comprehensive cross-clade neutralization analysis of a panel of anti-human immunodeficiency virus type 1 monoclonal antibodies. J. Virol. *78*, 13232–13252.

Brügger, B., Glass, B., Haberkant, P., Leibrecht, I., Wieland, I., Wieland, F.T., and Kräusslich, H.-G. (2006). The HIV lipidome: a raft with an unusual composition. Proc. Natl. Acad. Sci. USA *103*, 2641–2646.

Brunel, F.M., Zwick, M., Cardoso, R.M., Nelson, J.D., Wilson, I.A., Burton, D.R., and Dawson, P.E. (2006). Structure-function analysis of the epitope for 4E10, a broadly neutralizing human immunodeficiency virus type 1 antibody. J. Virol. *80*, 1680–1687.

Brunger, A.T. (1992). X-PLOR Version 3.1: A System for X-Ray Crystallography and NMR (New Haven, CT: Yale University Press).

Cardoso, R.M., Zwick, M.B., Stanfield, R.L., Kunert, R., Binley, J.M., Katinger, H., Burton, D.R., and Wilson, I.A. (2005). Broadly neutralizing anti-HIV antibody 4E10 recognizes a helical conformation of a highly conserved fusion-associated motif in gp41. Immunity *22*, 163–173.

Cardoso, R.M., Brunel, F.M., Ferguson, S., Zwick, M., Burton, D., Dawson, P.E., and Wilson, I.A. (2007). Structural basis of enhanced binding of extended and helically constrained peptide epitopes of the broadly neutralizing HIV-1 antibody 4E10. J. Mol. Biol. *365*, 1533–1544.

Centers for Disease Control and Prevention (CDC) (2006). The global HIV/AIDS pandemic, 2006. MMWR Morb. Mortal. Wkly. Rep. *55*, 841–844.

Chan, D.C., Fass, D., Berger, J.M., and Kim, P.S. (1997). Core structure of gp41 from the HIV envelope glycoprotein. Cell *89*, 263–273.

Chou, J.J., Kaufman, J.D., Stahl, S.J., Wingfield, P.T., and Bax, A. (2002). Micelle-induced curvature in a water-insoluble HIV-1 Env peptide revealed by NMR dipolar coupling measurement in stretched polyacrylamide gel. J. Am. Chem. Soc. *124*, 2450–2451.

Cornilescu, G., Delaglio, F., and Bax, A. (1999). Protein backbone angle restraints from searching a database for chemical shift and sequence homology. J. Biomol. NMR *13*, 289–302.

Dimitrov, A.S., Jacobs, A., Finnegan, C.M., Stiegler, G., Katinger, H., and Blumenthal, R. (2007). Exposure of the membrane-proximal external region of HIV-1 gp41 in the course of HIV-1 envelope glycoprotein-mediated fusion. Biochemistry *46*, 1398–1401.

Douek, D.C., Kwong, P.D., and Nabel, G.J. (2006). The rational design of an AIDS vaccine. Cell *124*, 677–681.

Epand, R.F., Thomas, A., Brasseur, R., Vishwanathan, S.A., Hunter, E., and Epand, R.M. (2006). Juxtamembrane protein segments that contribute to recruitment of cholesterol into domains. Biochemistry *45*, 6105–6114.

Farahbakhsh, Z.T., Altenbach, C., and Hubbell, W.L. (1992). Spin labeled cysteines as sensors for protein-lipid interaction and conformation in rhodopsin. Photochem. Photobiol. *56*, 1019–1033.

Feng, F., Broder, C.C., Kennedy, P.E., and Berger, E.A. (1996). HIV-1 entry co-factor: functional cDNA cloning of a seven-transmembrane, G protein-coupled receptor. Science *272*, 872–877.

Ferentz, A.E., and Wagner, G. (2000). NMR spectroscopy: a multifaceted approach to macromolecular structure. Q. Rev. Biophys. *33*, 29–65.

Guntert, P. (2004). Automated NMR structure calculation with CYANA. Methods Mol. Biol. *278*, 353–378.

Guntert, P., Dotsch, V., Wider, G., and Wuthrich, K. (1992). Processing of multidimensional NMR data with the new software PROSA. J. Biomol. NMR *2*, 619–629.

Han, Y., Wind-Rotolo, M., Yang, H.C., Siliciano, J.D., and Siliciano, R.F. (2007). Experimental approaches to the study of HIV-1 latency. Nat. Rev. Microbiol. *5*, 95–106.

Haynes, B.F., Fleming, J., St Clair, E.W., Katinger, H., Stiegler, G., Kunert, R., Robinson, J., Scearce, R.M., Plonk, K., Staats, H.F., et al. (2005). Cardiolipin polyspecific autoreactivity in two broadly neutralizing HIV-1 antibodies. Science *308*, 1906–1908.

Hollis, T., Ichikaw, Y., and Ellenberger, T. (2000). DNA binding and a flip-out mechanism for base excision by the helix-hairpin-helix DNA glycosylase, *Escherichia coli* AlkA. EMBO J. *19*, 758–766.

Hubbell, W.L., Gross, A., Langen, R., and Lietzow, M.A. (1998). Recent advances in site-directed spin labeling of proteins. Curr. Opin. Struct. Biol. *8*, 649–656.

Ihaka, R., and Gentleman, R. (1996). R: a language for data analysis and graphics. J. Comput. Graph. Statist. *3*, 299–314.

Keller, R.L.J. (2004). The Computer and Resonance Assignment Tutorial, First Edition (Goldau, Switzerland: Cantina Verlag).

Kim, M., Qiao, Z., Yu, J., Montefiori, D., and Reinherz, E.L. (2007). Immunogenicity of recombinant human immunodeficiency virus type 1-like particles expressing gp41 derivatives in a pre-fusion state. Vaccine *25*, 5102–5114.

Korber, B., Gaschen, B., Yusim, K., Thakallapally, R., Kesmir, C., and Detours, V. (2001). Evolutionary and immunological implications of contemporary HIV-1 variation. Br. Med. Bull. *58*, 19–42.

Law, M., Cardoso, R.M., Wilson, I.A., and Burton, D.R. (2007). Antigenic and immunogenic study of membrane-proximal external region-grafted gp120 antigens by a DNA prime-protein boost immunization strategy. J. Virol. *81*, 4272–4285.

Letvin, N.L. (2006). Progress and obstacles in the development of an AIDS vaccine. Nat. Rev. Immunol. *6*, 930–939.

Li, M., Gao, F., Mascola, J.R., Stamatatos, L., Polonis, V.R., Koutsoukos, M., Voss, G., Goepfert, P., Gilbert, P., Greene, K.M., et al. (2005). Human immunodeficiency virus type 1 env clones from acute and early subtype B infections for standardized assessments of vaccine-elicited neutralizing antibodies. J. Virol. *79*, 10108–10125.

Lorizate, M., Cruz, A., Huarte, N., Kunert, R., Perez-Gil, J., and Nieva, J.L. (2006). Recognition and blocking of HIV-1 gp41 pre-transmembrane sequence by monoclonal 4E10 antibody in a Raft-like membrane environment. J. Biol. Chem. *281*, 39598–39606.

Munoz-Barroso, I., Salzwedel, K., Hunter, E., and Blumenthal, R. (1999). Role of the membrane-proximal domain in the initial stages of human immunodeficiency virus type 1 envelope glycoprotein-mediated membrane fusion. J. Virol. *73*, 6089–6092.

Nelson, J.D., Brunel, F.M., Jensen, R., Crooks, E.T., Cardoso, R.M.F., Wang, M., Hessell, A., Wilson, I.A., Binley, J.M., Dawson, P.E., et al. (2007). An affinity-enhanced neutralizing antibody against the membrane-proximal external region of human immunodeficiency virus type 1 (HIV-1) gp41 recognizes an epitope between those of 2F5 and 4E10. J. Virol. *81*, 4033–4043.

Ofek, G., Tang, M., Sambor, A., Katinger, H., Mascola, J.R., Wyatt, R., and Kwong, P.D. (2004). Structure and mechanistic analysis of the anti-human immunodeficiency virus type 1 antibody 2F5 in complex with its gp41 epitope. J. Virol. *78*, 10724–10737.

Oh, K.J., Altenbach, C., Collier, R.J., and Hubbell, W.L. (2000). Site-directed spin labeling of proteins. Applications to diphtheria toxin. Methods Mol. Biol. *145*, 147–169.

Pervushin, K. (2000). Impact of transverse relaxation optimized spectroscopy (TROSY) on NMR as a technique in structural biology. Q. Rev. Biophys. *33*, 161–197.

Popova, A.V., Heyer, A.G., and Hincha, D.K. (2002). Differential destabilization of membranes by tryptophan and phenylalanine during freezing: the roles of a lipid composition and membrane fusion. Biochim. Biophys. Acta *1561*, 109–118.

Qiao, Z., Kim, M., Reinhold, B., Montefiori, D., Wang, J.-H., and Reinherz, E.L. (2005). Design, expression and immunogenicity of a soluble HIV trimeric envelope fragment adopting a prefusion gp41 configuration. J. Biol. Chem. *280*, 23138–23146.

Salzwedel, K., West, J.T., and Hunter, E. (1999). A conserved tryptophan-rich motif in the membrane-proximal region of the human immunodeficiency virus

type 1 gp41 ectodomain is important for Env-mediated fusion and virus infectivity. J. Virol. *73*, 2469–2480.

Schibli, D.J., Montelaro, R.C., and Vogel, H.J. (2001). The membrane-proximal tryptophan-rich region of the HIV glycoprotein, gp41, forms a well-defined helix in dodecylphosphocholine micelles. Biochemistry *40*, 9570–9578.

Schwieters, C.D., Kuszewski, J.M., Tjandra, N., and Clore, G.M. (2003). The Xplor-NIH NMR molecular structure determination package. J. Magn. Reson. *160*, 66–74.

Shimada, I. (2005). NMR techniques for identifying the interface of a larger protein-protein complex: cross-saturation and transferred cross-saturation experiments. Methods Enzymol. *394*, 483–506.

Shin, Y.K., and Hubbell, W.L. (1992). Determination of electrostatic potentials at biological interfaces using electron-electron double resonance. Biophys. J. *61*, 1443–1453.

Suárez, T., Nir, S., Goñi, F.M., Saéz-Cirión, A., and Nieva, J.L. (2000). The pre-transmembrane region of the human immunodeficiency virus type-1 glycoprotein: a novel fusogenic sequence. FEBS Lett. *477*, 145–149.

Xu, Y.-Y., Gorny, M.K., Palker, T., Karwowska, S., and Zolla-Pazner, S. (1991). Epitope mapping of two immunodominant domains of gp41, the transmembrane protein of human immunodeficieincy virus type 1, using ten human monoclonal antibodies. J. Virol. *65*, 4832–4838.

Yuste, E., Sanford, H., Carmody, J., Bixby, J., Little, S., Zwick, M., Greenough, T., Burton, D., Richman, D.D., Desrosiers, R.C., and Johnson, W.E. (2006). Simian immunodeficiency virus engrafted with human immunodeficiency virus type 1 (HIV-1)-specific epitopes: replication, neutralization, and survey of HIV-1-positive plasma. J. Virol. *80*, 3030–3041.

Zanetti, G., Briggs, J.A.G., Grunewald, K., Sattentau, Q.J., and Fuller, S.D. (2006). Cryo-electron tomographic structure of an immunodeficiency virus envelope complex in situ. PLoS Pathog. *2*, e83. 10.1371/journal.ppat.0020083.

Zhu, P., Liu, J., Bess, J.J., Chertova, E., Lifson, J.D., Grise, H., Ofek, G.A., Taylor, K.A., and Roux, K.H. (2006). Distribution and three-dimensional structure of AIDS virus envelope spikes. Nature *441*, 847–852.

Zwick, M.B., Jensen, R., Church, S., Wang, M., Stiegler, G., Kunert, R., Katinger, H., and Burton, D.R. (2005). Anti-human immunodeficiency virus type 1 (HIV-1) antibodies 2F5 and 4E10 require surprisingly few crucial residues in the membrane-proximal external region of glycoprotein gp41 to neutralize HIV-1. J. Virol. *79*, 1252–1261.

Accession Numbers

The PDB accession number for the NMR structures is 2pv6.